Burns & Trauma, 2024, 12, tkae018
https://doi.org/10.1093/burnst/tkae018
Research Article

OXFORD

Research Article

Engineered nanovesicles from activated neutrophils with enriched bactericidal proteins have molecular debridement ability and promote infectious wound healing

Hangfei Jin[†], Xiao Wen[†], Ran Sun[†], Yanzhen Yu, Zaiwen Guo, Yunxi Yang, Linbin Li and Bingwei Sun*[*]

Research Center for Neutrophil Engineering Technology, Affiliated Suzhou Hospital of Nanjing Medical University, located at No. 242, Guangji Road, Gusu District, Suzhou 215008, Jiangsu Province, China

[*]Correspondence. sunbinwe@hotmail.com

[†]Hangfei Jin, Xiao Wen and Ran Sun contributed equally to this work.

Received 20 December 2023; Revised 22 February 2024; Accepted 27 March 2024

Abstract

Background: Bacterial infections pose a considerable threat to skin wounds, particularly in the case of challenging-to-treat diabetic wounds. Systemic antibiotics often struggle to penetrate deep wound tissues and topically applied antibiotics may lead to sensitization, necessitating the development of novel approaches for effectively treating germs in deep wound tissues. Neutrophils, the predominant immune cells in the bloodstream, rapidly release an abundance of molecules via degranulation upon activation, which possess the ability to directly eliminate pathogens. This study was designed to develop novel neutrophil cell engineered nanovesicles (NVs) with high production and explore their bactericidal properties and application in promoting infectious wound healing.

Methods: Neutrophils were isolated from peripheral blood and activated *in vitro* via phorbol myristate acetate (PMA) stimulation. Engineered NVs were prepared by sequentially extruding activated neutrophils followed by ultracentrifugation and were compared with neutrophil-derived exosomes in terms of morphology, size distribution and protein contents. The bactericidal effect of NVs *in vitro* was evaluated using the spread plate technique, LIVE/DEAD backlight bacteria assay and observation of bacterial morphology. The therapeutic effects of NVs *in vivo* were evaluated using wound contraction area measurements, histopathological examinations, assessments of inflammatory factors and immunochemical staining.

Results: Activated neutrophils stimulated with PMA *in vitro* promptly release a substantial amount of bactericidal proteins. NVs are similar to exosomes in terms of morphology and particle size, but they exhibit a significantly higher enrichment of bactericidal proteins. *In vitro*, NVs demonstrated a significant bactericidal effect, presumably mediated by the enrichment of bactericidal proteins such as lysozyme. These NVs significantly accelerated wound healing, leading to a marked reduction in bacterial load, downregulation of inflammatory factors and enhanced collagen deposition in a full-thickness infectious skin defect model.

Conclusions: We developed engineered NVs derived from activated neutrophils to serve as a novel debridement method targeting bacteria in deep tissues, ultimately promoting infectious wound healing.

Graphical Abstract

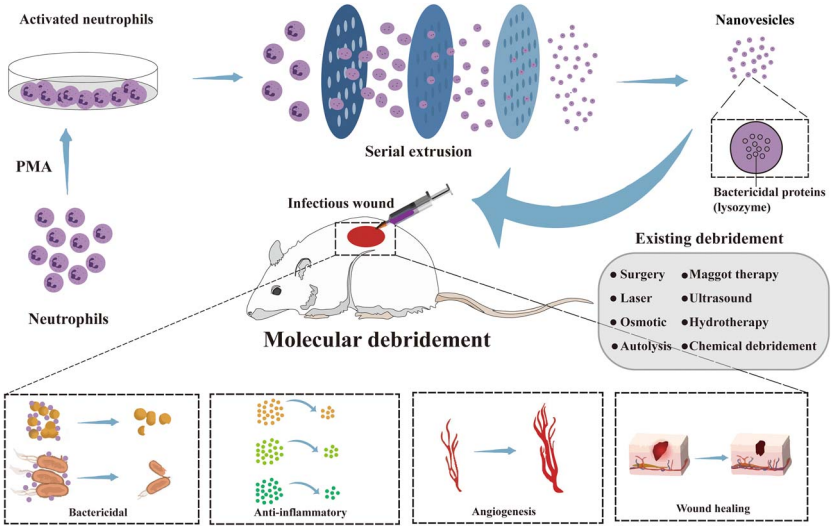

Key words: Neutrophil, Engineered nanovesicles, Molecular debridement, Bactericidal proteins, Infectious wound

Highlights

- Neutrophils can rapidly release an abundance of molecules to eliminate pathogens.
- Engineered nanovesicles were successfully generated from activated neutrophils.
- Engineered nanovesicles were enriched with bactericidal proteins such as lysozyme.
- Engineered nanovesicles selectively target inflamed deep tissues for the treatment of bacterial-induced infectious wounds.
- Nanovesicles significantly accelerated wound healing.

Background

Wound healing challenges not only impose a substantial economic burden on healthcare systems worldwide but also significantly diminish the quality of life for patients [1]. Infections represent one of the most common hurdles to wound healing [2], with antibiotics being the primary treatment approach [3]. However, systemic antibiotics struggle to effectively reach deep wound tissues, and topically applied antibiotics often lead to sensitisation [4]. Moreover, excessive antibiotic use can result in severe cytotoxicity and the emergence of bacterial resistance, further complicating the treatment of infected wounds [5]. Debridement can be achieved through mechanical, sharp, surgical, autolytic, enzymatic or biological methods [6]. Microorganisms within wound tissue produce an extracellular matrix comprising proteins, polysaccharides and DNA, which enhances adhesion to the wound site [7]. Traditional debridement techniques, such as mechanical debridement, struggle to completely eliminate this biofilm and may inadvertently damage healthy tissue. Consequently, there is an urgent need for innovative debridement approaches to expedite the healing of infected wounds.

Neutrophils, the predominant immune cells circulating in the blood, are the first responders to infection sites [8]. Neutrophils are the first circulating inflammatory cells recruited to the wound site, and their main role is to clear foreign debris and defend against possible infections [9,10]. When activated by inflammation, these neutrophils can rapidly release a plethora of molecules via degranulation, which possess the ability to directly combat pathogens [11]. Exosomes (Exos), specialized differentiated vesicles of cells, measuring 50 to 200 nm in diameter, play a pivotal role in the intercellular transport of these molecules and proteins [12]. Moreover, Exos offer distinct advantages, such as extended circulation, evasion of phagocytosis, and deep tissue penetration, making them promising candidates for drug delivery [13]. However, isolating Exos is challenging due to their limited release in small quantities, and the purification process is both time-consuming and intricate [14].

To address these yield limitations, cell-engineered nanovesicles (NVs) have emerged as a promising alternative to Exos for drug delivery. Engineered NVs are mechanically created by repeatedly passing cells through a microporous filter. This process fragments the cell membrane, allowing it to spontaneously reassemble into nanoscale vesicles [15], retaining a significant portion of the source cell's proteins and RNA. As a substitute for Exos, engineered NVs not only replicate the cellular functions but also overcome the challenges of limited exosome availability and purification difficulties [16].

In this study, we generated engineered NVs from activated neutrophils for the treatment of infectious skin wounds. We initially compared the bactericidal effects of engineered NVs with Exos derived from neutrophils incubated with bacteria *in vitro*. Engineered NVs showed significant bactericidal activity. Furthermore, the *in vivo* therapeutic effects of NVs were evaluated using wound contraction area measurements, histopathological examinations, assessments of inflammatory factors and immunochemical staining. All results pointed to the considerable potential of these activated neutrophil-engineered NVs, which exhibit remarkable bactericidal properties, especially for the management of infectious skin wounds.

Methods

Ethical statement

This study received approval from the Medical Ethical Committee of Suzhou Municipal Hospital (KL901390). Blood specimens were collected from the cubital veins of healthy drug-free donors who provided written informed consent before participating. All experimental procedures were conducted in strict compliance with approved guidelines. All experimental procedures involving rats and mice were carried out in strict accordance with the recommendations outlined in the Guide for the Care and Use of Laboratory Animals of the National Institutes of Health and State Key Laboratory of Pathogens and Biosecurity of the Institute of Microbiology and Epidemiology.

Extraction and activation of human neutrophils

Peripheral blood was collected from healthy volunteers using EDTAK2 anticoagulant tubes, and neutrophils were isolated from the peripheral blood using the EasySep™ direct human neutrophil isolation kit (Stemcell, 19 666). Neutrophils were cultured in a 37.5°C incubator with 5% CO_2 using RPMI1640 medium (Gibco, 11 875 119) containing 10% exosome-free fetal bovine serum (OPCEL, BS-1205) and 1% penicillin and streptomycin (Beyotime, C0222). The neutrophils were activated by stimulation with 100 nM phorbol myristate acetate (PMA; MedChemExpress, HY-18739) and incubated at 37.5°C for 30 min.

Immunostaining and microscopy

Cells were fixed in 4% paraformaldehyde, permeabilized with 0.1% Triton X-100 (Beyotime, P0096-100 ml), blocked with 5% Bovine Serum Albumin (BSA; Beyotime, ST025-20 g) and then stained with 4′,6-diamidino-2-phenylindole dihydrochloride (DAPI; Solarbio, D6470) and Phalloidin-iFluor 488 (Abcam, ab176753). Stained neutrophils were observed using a Zeiss LSM 900 confocal microscope.

Flow cytometry detection

Neutrophils were incubated at room temperature for 30 min with anti-CD66b (BD Biosciences, 555 723), anti-CD35 (BD Biosciences, 555 451) and anti-CD63 (BD Biosciences, 561 983). Cells were washed twice in phosphate buffered saline (PBS; Gibco, 20012027) and analysed for fluorescence intensity using flow cytometry.

Enzyme-Linked immunosorbent assay

After neutrophils were stimulated with PMA, the culture supernatant was collected. The Enzyme-Linked immunosorbent assay (ELISA) was conducted based on a kit protocol (RD, DY9167–05, DY3174; Elabscience, E-EL-H1869C). 100-μl volumes of standards or samples were added to a 96 well plate and incubated at room temperature. Three wells were allocated for each sample. Subsequently, biotinylated antibody, streptavidin–horseradish peroxidase reagent and 3, 3′, 5, 5′-Tetramethylbenzidine substrate were added to the wells in accordance with the protocol. The plate was developed at room temperature in the dark until a noticeable colour change occurred, and then a stop solution was added to each well. The absorbance was measured at 450 nm within 5 min and the data were recorded. A standard curve was constructed, and the corresponding concentration was determined.

Preparation of engineered NVs

The suspension of activated neutrophils was passed 11 times through filter membranes (Whatman) with decreasing apertures (8, 5, 1, 0.4 and 0.2 μm) using a mini-extruder (Avanti Polar Lipids). The extruding fluid was centrifuged for 30 min at 3000 × g to remove cell membrane fragments. Thereafter, it was centrifuged at 100,000 × g for 90 min at 4°C to collect the NVs. The final NVs pellet was resuspended in PBS and stored at −80°C until use.

Collection of Exos

Neutrophils were cultured in an exosome-free medium for 24 h. Then, the cells were removed by centrifugation at 400 × g for 7 min, and apoptotic bodies and large cell debris were eliminated by centrifuging at 2000 × g for 10 min. Large microvesicles were isolated by centrifugation at 10,000 × g for 30 min, followed by purification through ultracentrifugation at 100,000 × g for 70 min. The Exos were dissolved in PBS and stored at −80°C until use.

Characterization and analysis of NVs and Exos

A transmission electron microscope (TEM, Joel 10 011, Japan) was used to determine the purity of the NVs and Exos. The purified NVs and Exos were placed onto a formvar/carbon-coated grid, rinsed after a 30-min absorption period and negatively stained with 2% uranyl acetate. The TEM grid was examined after drying. Size and particle concentration of NVs and Exos were determined using a nanoparticle tracking analysis instrument (NanoSight, Malvern Instruments) equipped with a blue laser (405 nm).

Western blot

NVs and Exos were lysed using Radio Immunoprecipitation Assay Lysis buffer (Beyotime, P0013B) and the supernatant

from lysates was used for subsequent western blot analysis. Protein samples were separated by 10% sodium dodecyl sulfate-polyacrylamide gel electrophoresis and then transferred onto a Polyvinylidene Fluoride membrane (Beyotime, FFP22). After blocking in Tris-Buffered saline with tween 20 (TBST) with 5% non-fat milk for 2 h, membranes were incubated at 4°C overnight with the following primary antibodies: CD63 (ImmunoWay Biotechnology, YT5525), tumour susceptibility gene 101 (TSG101; ImmunoWay Biotechnology, YT4760), Alix (Wuhan Sanying,12 422–1-AP), calnexin (Wuhan Sanying,10 427–2-AP) and lysozyme (Wuhan Sanying,15 013–1-AP). The next day, membranes were washed with TBST and incubated with horseradish peroxidase-conjugated goat anti-rabbit (Abways Technology, AB0101) and anti-mouse (Abways Technology, AB0102) IgG antibodies for 2 h at room temperature. Finally, bands were visualized using enhanced chemiluminescent blotting detection reagents.

NVs bactericidal assay *in vitro*

Staphylococcus aureus and *Escherichia coli* bacterial suspensions (100 μl; 10^7 Colony Forming Units/ml; CFU/ml) were incubated with 2 ml of PBS, Exos (40 μg/ml) and NVs (40 μg/ml) at 37°C for 2 h. Subsequently, 100 μl of the bacterial solution was evenly distributed on an Luria-Bertani (LB) agar plate and incubated at 37°C for 16 h, followed by bacterial colony counting.

LIVE/DEAD backlight bacteria assay

The treated bacteria were stained with a LIVE/DEAD backlight bacterial viability kit containing Dimethylaminophenoxazine Oxide (DMAO) and Ethidium Homodimer 3 (EthD-III) (YEASEN, 40274ES60). Then, 5 μl of bacterial suspension was smeared on a glass slide and images were captured using a Zeiss LSM 900 confocal microscope.

Bacterial morphology

A SEM was employed to observe and assess bacterial morphology. Bacteria treated with different methods were centrifuged at 10,000 rpm for 3 min, washed with PBS, fixed with electron microscope fixative, dried using freeze-drying, gold-sprayed and observed under a SEM (Model, Verios G4, USA).

Proteomics

Protein analysis was conducted using a label-free quantitative technique based on mass spectrometry. In brief, Exos and NVs were solubilized in lysis buffer (50 mM Tris buffer, 8 M urea, 1% SDS, pH 8) and sonicated on ice for 5 min. The lysate was centrifuged at 13,000 rpm for 20 min at 4°C and the supernatant was treated with 4-fold acetone (containing 10 mM Dithiothreitol) for 2 hours. The resulting protein sample was collected by centrifugation and evaporated. The protein sample was further digested, desalted and lyophilized for Liquid Chromatography-Tandem Mass Spectrometry analysis. Peptides were separated from the lyophilized powder and analysed using a Q Exactive TM HF-X mass spectrometer (Thermo Fisher), with an ion source of Nanospray Flex™ (ESI). The raw MS files were analysed and searched against the human protein database. All acquired spectra were searched using Proteome Discoverer (PD) 2.2 (Thermo). The parameters for PD 2.2 were set as follows: precursor ion and product ion mass tolerances of 10 ppm and 0.02 Da, respectively. Carbamidomethyl, oxidation of methionine (M) and acetylation were specified as fixed modifications, dynamic modifications and N-terminal modifications, respectively. A maximum of two missed cleavages was allowed. To enhance the quality of the analysis, the search results were further filtered: Peptide Spectrum Matches (PSMs) with a confidence > 99% were identified as reliable. Identified proteins included at least one unique peptide segment. The identified PSMs and proteins were recorded and the False Discovery Rate did not exceed 1.0%. Protein quantification results were statistically analysed using a t-test. Proteins with significant differences in quantity between the experimental group and the control group ($P < 0.05$ and $|\log2FC| > *$ [$FC > *$ or $FC < *$ (where FC is fold change)] were defined as differentially expressed proteins.

Diabetic rat and mouse infected wound models

To induce a type 2 diabetic rat model, Sprague–Dawley male rats (6 weeks old) were fed a high-fat diet for 4 weeks, followed by a 24-h fast and intraperitoneal injections with 40 mg/kg streptozotocin (STZ) (10 mg/ml). One week later, the blood glucose level of the rats was measured to be >16.7 mmol/l, confirming the successful establishment of the diabetic rat model [17].

To induce a type 2 diabetic mouse model, C57 male mice (6–8 weeks old) were fed a high-fat diet for 14 days, followed by a 24-h fast and intraperitoneal injections of 50 mg/kg STZ (10 mg/ml) for 5 consecutive days. One week later, the blood glucose level of the mice was measured to be >16.7 mmol/l, indicating the successful establishment of the diabetic mouse model.

In vivo bactericidal activity of NVs

The rats were randomly divided into three groups (six rats per group) and anaesthetized with isoflurane (RWD). Subsequently, circular wounds with a diameter of 10 mm were made on the back of each rat. These wounds were then infected with 10^7 CFU of *S. aureus*. One day later, the diabetic rat infection model was established and the wounds were treated with 1 ml of PBS (control group), 1 ml of 40 μg/ml Exos (Exos group) and 1 ml of 40 μg/ml NVs (NVs group) (day 0).

The mice were randomly divided into three groups (six mice per group) and anaesthetized with isoflurane (RWD). Subsequently, circular wounds with a diameter of 10 mm were made on the back of each mouse and the wounds were infected with 10^7 CFU of *S. aureus*. One day later, the

diabetic mice infection model was established. The wounds were treated with 1 ml of PBS (control group), 1 ml of 40 μg/ml Exos (Exos group) and 1 ml of 40 μg/ml NVs (NVs group) (day 0).

Real-time quantitative polymerase chain reaction

All primers used for mRNA detection were synthesized by Suzhou Genewiz Biotech. Table 1 shows the sequences of all primers in this study. Real-time quantitative polymerase chain reaction (qRT-PCR) was performed using AceQ Universal SYBR qPCR Master Mix (Vazyme) following the manufacturer's protocol. The reaction volumes comprised 5 μl of diluted cDNA solution, 10 μl Mastermix, and 0.4 μl each of forward and reverse primers. StepOnePlus™ Real-Time PCR System was used for thermal cycling (Applied Biosystems) with the following thermocycling conditions: denaturation at 95°C for 5 min, followed by 40 cycles of 95°C for 10 s and 60°C for 30 s. microRNA expression was normalized to U6 microRNA and calculated using the $2^{-\Delta\Delta CT}$ method.

Determination of inflammatory cytokine contents using cytometric bead array

A BD cytometric bead array (CBA) mouse Th1/Th2/Th17 cytokine kit (Cat#560485) was used as described to assess the concentrations of interleukin 2 (IL-2), IL-4, IL-6, IL-10, IFN-γ, tumour necrosis factor (TNF) and IL-17A in plasma. All related reagents, flow cytometry protocols and result analyses were performed in accordance with the kit instructions. Standard curves of inflammatory cytokines were prepared. The capture beads for these seven inflammatory cytokines were mixed rigorously to create a bead mixture. Subsequently, 50 μl of this mixture was added to each sample, followed closely by the addition of 50 μl of PE detection reagent. All array tubes were incubated for 2 h at room temperature and shielded from light. The array tubes were rinsed once with wash buffer, centrifuged and resuspended before flow cytometry analysis. A BD LSR Fortessa Multicolor Flow Cytometer was used for examination. Experimental results were analysed using FCAP Array v3.1, FlowJo v10.4 and CurveExpert v1.4.

Statistical analysis

All statistical analyses were performed and graphs were prepared with GraphPad Prism 8.0 software and Adobe Illustrator. The Shapiro–Wilk test was used to test the normality of continuous variables. The results are expressed as the mean ± standard deviation (SD). For group comparisons, one-way analysis of variance was used to compare continuous variables with a normal distribution. The Kruskal–Wallis test was used to compare continuous variables with a skewed distribution. Tukey's *post hoc* test or Dunn's *post hoc* test was used for multiple comparisons. Students t test and the Wilcoxon paired signed rank test were used to compare differences between two groups. The Pearson correlation coefficient was used for correlation analysis. Significant differences are noted by asterisks ($^{*}P < 0.05$, $^{**}P < 0.01$, $^{***}P < 0.001$, $^{****}P < 0.0001$).

Results

Activated neutrophils release substantial amounts of bactericidal proteins

Neutrophils were isolated and purified from healthy adult volunteers using magnetic beads and activated with PMA (Figure 1a). PMA, a phorbol ester compound derived from the plant *Croton tiglium*, is widely used in experiments to activate neutrophils [18]. Confocal images revealed that, in contrast to the scattered distribution of normal neutrophils, activated neutrophils exhibited adhesion to each other and a change in the shape of their nuclei (Figure 1b). Compared with normal neutrophils, the chemotactic function of activated neutrophils is significantly decreased (Figure S1, see online supplementary material), but its phagocytosis is enhanced (Figure S2a, b, see online supplementary material). Flow cytometry demonstrated a significant increase in the expression of CD66b in activated neutrophils (Figure 1c). These results confirm the successful isolation and activation of neutrophils. Activated neutrophils combat invading pathogens by releasing bactericidal proteins through degranulation [19]. Flow cytometric analysis of CD63 and CD35 displayed a clear increase in degranulation for activated neutrophils (Figure 1d, e). ELISA experiment results indicated a significant increase in neutrophil elastase and lysozyme levels in the culture medium of activated neutrophils, signifying the release of a substantial quantity of bactericidal proteins (Figure 1f, g and Figure S2c, see online supplementary material).

Generation and characterization of engineered NVs from activated neutrophils

Exos were isolated by differential ultracentrifugation from an Exos-free culture medium for neutrophils. Engineered NVs were prepared using a sequential extrusion method involving the extrusion of activated neutrophils, along with bactericidal

Table 1. Primers used for RT-qPCR analysis

Gene	Species	Sequence (5′to 3′)
IL-1β	Rat	Forward: 5′-GTTTGAGTCTGCACAGTTCCC-3′
		Reverse: 5′-AAGTCAACTATGTCCCGACCA-3′
IL-6	Rat	Forward: 5′-TGAAGTTTCTCTCCGCAAG-3′
		Reverse: 5′-TATGTAATTAAGCCTCCGACT-3′
TNF-α	Rat	Forward: 5′-GCCTCTTCTCATTCCTGCTCGT-3′
		Reverse: 5′-TTCTCCTCCTTGTTGGGACCGAT-3′
GAPDH	Rat	Forward: 5′-ATGACTCTACCCACGGCAAG-3′
		Reverse: 5′- GACGCCAGTAGACTCCACGAC-3′

IL-1β interleukin 1 beta, *TNF-α* tumour necrosis factor-alpha, *GAPDH* glyceraldehyde-3-phosphate dehydrogenase

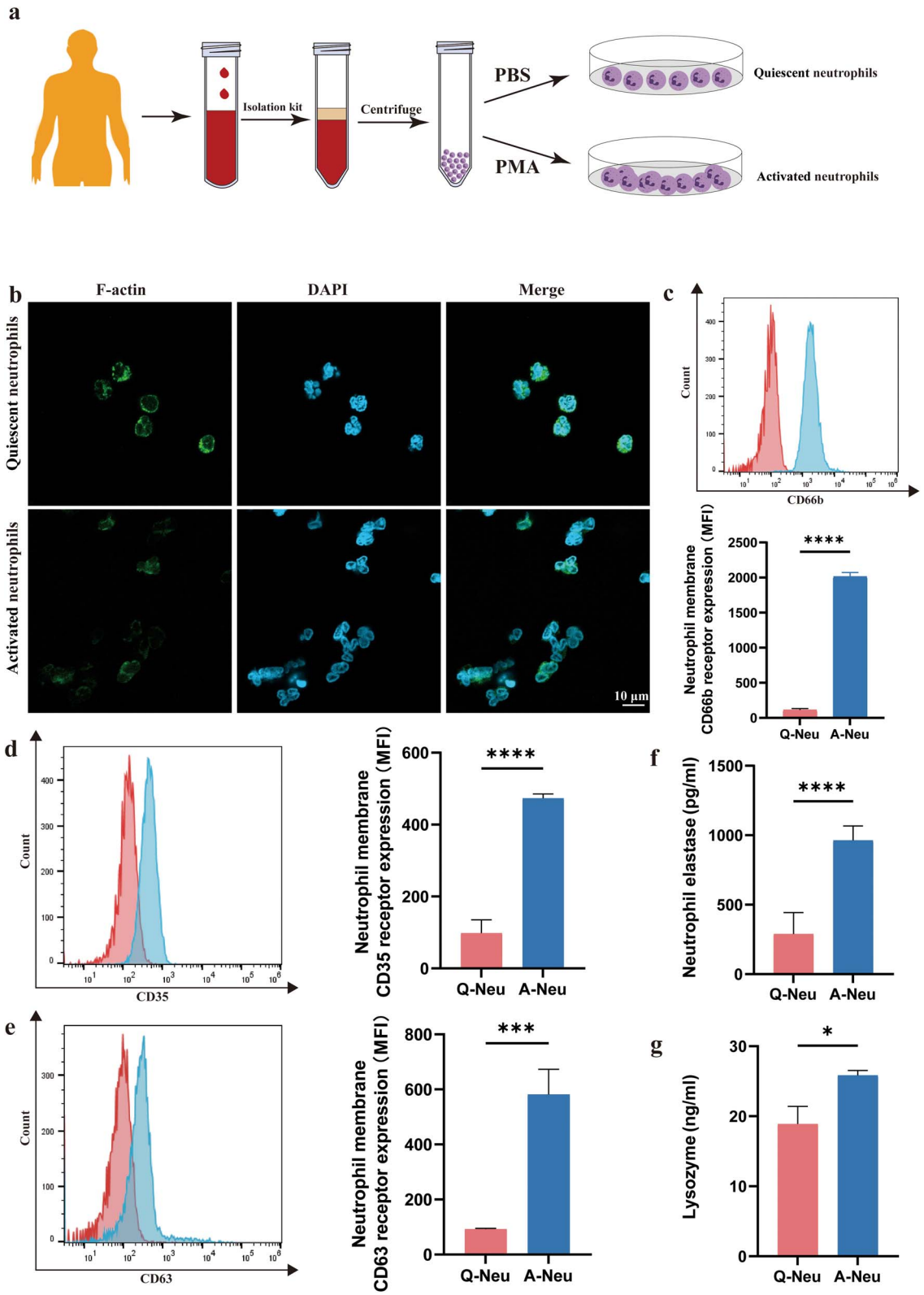

Figure 1. Activated neutrophils release of bactericidal proteins. (**a**) Schematic representation of the isolation and activation of human neutrophils. (**b**) Fixed neutrophils with rhodamine-labelled F-actin, DAPI-labelled nucleus and merged images (scale bar: 10 μm). (**c**) Increased expression of CD66b on activated neutrophils (n = 3). (**d**, **e**) Enhanced expression of CD35 and CD63 on activated neutrophils (n = 3). (**f**, **g**) Elevated concentrations of neutrophil elastase and lysozyme in the culture medium of activated neutrophils detected by ELISA (n = 3). Data are presented as mean ± SD. $^{*}p < 0.05$, $^{***}p < 0.001$, $^{****}p < 0.0001$. *PBS* phosphate buffered saline, *PMA* phorbol myristate acetate, *Q-Neu* quiescent neutrophils, *A-Neu* activated neutrophils, *MFI* mean fluorescence intensity

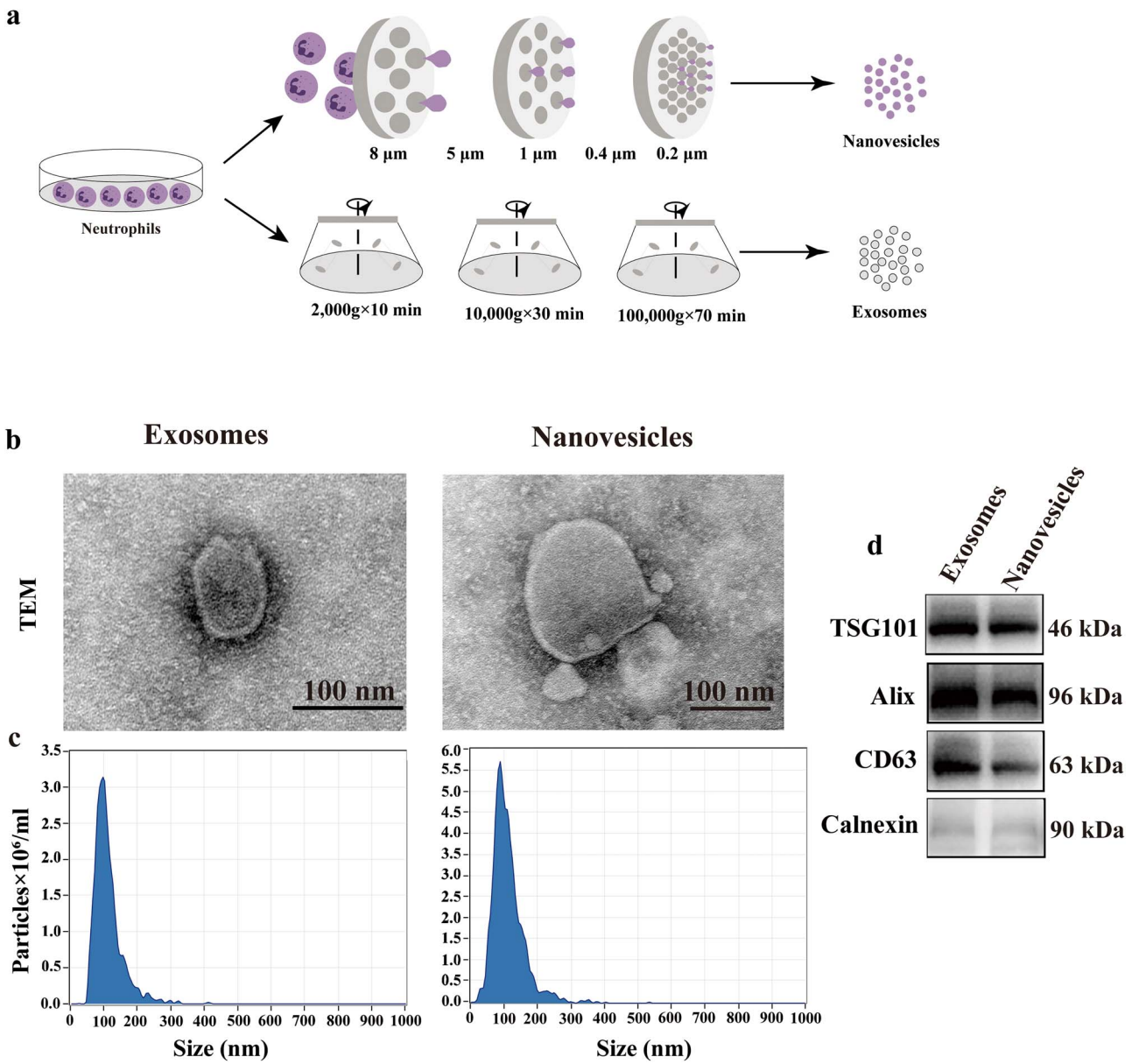

Figure 2. Generation and characterization of engineered nanovesicles (NVs) from activated neutrophils. (**a**) Schematic illustration of NV and exosome preparation. (**b**) TEM images of NVs and exosomes (Exos) (scale bar: 100 nm). (**c**) Nanoparticle tracking analysis of NVs and Exos, showing a peak diameter ranging between 50 and 150 nm. (**d**) Western blot analysis of TSG101, Alix, CD63 and calnexin protein expression in NVs and Exos. *TSG101* tumour susceptibility gene 101

protein cultures, through polycarbonate membrane microfilters with progressively decreasing apertures (8, 5, 1, 0.4 and 0.2 μm), followed by ultracentrifugation (Figure 2a). The morphology, size distribution and protein contents of purified Exos and NVs were assessed. TEM images revealed that NVs consisted of ~100 nm spherical vesicles enclosed by a bilayer lipid membrane, resembling the known morphology of Exos (Figure 2b). Nanoparticle tracking analysis of Exos and NVs confirmed a similar size distribution, with a central diameter ranging between 50 and 150 nm (Figure 2c). To confirm the isolated NVs and Exos, western blotting was used to assess the typical extracellular vesicle proteins. Both NVs and Exos displayed the presence of tumour susceptibility gene 101 (TSG101), the transmembrane protein CD63 and cytosolic protein Alix, while no expression of calnexin was detected (Figure 2d).

Bactericidal effect by NVs *in vitro*

To investigate the bactericidal effect of NVs and Exos, both were administered to the same initial number of *S. aureus* and *E. coli*. The counting of bacterial colonies revealed that NVs treatment effectively inhibited the growth of *S. aureus* and *E. coli in vitro* (Figure 3a–d). We then used DMAO and an EthD-III live/dead fluorescent staining assay to analyse the membrane integrity of *S. aureus* and *E. coli* with different treatments. It is well known that DMAO is commonly used to

stain cells and can stain both living and dead cells, whereas EthD-III specifically stains dead or injured cells [20]. Only green fluorescence was observed in the control and Exos groups, indicating intact cell membranes of *S. aureus* and *E. coli*. In contrast, treatment with NVs resulted in a substantial overlap of green and red fluorescence (Figure 3e, f), suggesting that NVs disrupt the cell membranes of *E. coli* and *S. aureus*. To assess the bactericidal effect of NVs, a SEM was used to monitor the morphological changes in *S. aureus* and *E. coli*. In the control and Exos groups, both *E. coli* and *S. aureus* exhibited smooth surfaces with intact cell walls. In contrast, treatment with NVs led to obvious depressions on the bacterial surface, complete disruption of the bacterial membrane and severe damage to the inherent bacterial morphology (Figure 3g, h).

Proteomic analysis of NVs and Exos

To elucidate the functional molecules mediating the bactericidal effects of NVs, we conducted a proteomic analysis using Labfree technology to detect the protein expression profiles in NVs and Exos. In total, 4205 protein groups were identified, with 3705 proteins quantified. Differentially expressed proteins were identified using a cut-off of absolute FC $\geq$ 1.5 and *P*-value $<$ 0.05. The results indicated that 1807 proteins exhibited differential expression between NVs and Exos. Among these, 1501 proteins in NVs had significantly higher expression, while 306 proteins exhibited lower expression than in Exos (Figure 4a, b). These differential proteins were mainly located in the nucleus, cytoplasm and extracellular region (Figure S3a, see online supplementary material). Subsequently, we bioinformatically interpreted the differentially expressed proteins and explored the biological processes in which they were involved. Gene Ontology enrichment analysis revealed that NVs had similar biological processes, cellular components and molecular functions to Exos (Figure S3b, see online supplementary material). We also analyzed the Kyoto Encyclopedia of Genes and Genomes (KEGG) Pathway high expression of differential proteins (Figure S3c, see online supplementary material). The findings demonstrated that NVs were enriched in proteins associated with the regulation of multiple biological processes related to bacterial infectious diseases (Figure 4c). The expression ratio of a class of bactericidal-related proteins in NVs was higher compared to Exos (Figure 4d). Notably, lysozyme, an essential bactericidal protein for host defence, was up-regulated 4.39-fold in NVs compared to Exos. The results of western blotting confirmed the enrichment of lysozyme in NVs and Exos (Figure 4e, f). We tested the antibacterial effect of lysozyme (50 μg/ml) on *S. aureus* (Figure S3d, see online supplementary material).

NVs exhibit bactericidal and anti-inflammatory effects in the acute phase of infectious wound healing

To demonstrate the infectious wound healing effects of prepared NVs *in vivo*, bacterial infected trauma was induced in the dorsal skin of rats. PBS and Exos were used as comparisons (Figure 5a). After various treatments, wound images were captured at 0, 3, 7 and 15 days, respectively. Over time, all wound areas were reduced in size. Particularly, the NVs-treated group exhibited nearly complete wound healing after 15 days (Figure 5b–d). By collecting and homogenizing the skin tissue from the wound areas on day 2, bactericidal performance was evaluated (Figure 5e, f). The wounds treated with NVs showed the fewest bacterial colonies, indicating effective bactericidal action in deep tissue. Expression of inflammatory factors in wound tissues was assessed at 24 and 48 h to evaluate the anti-inflammatory performance of NVs (Figure 5g, h). Expression of IL-1β, TNF-α and IL-6 in the NVs group was significantly lower than in the control and Exos groups, indicating that NVs reduced inflammation at the wound site after 48 h. Plasma samples from infected wound models of diabetic mice were analysed for changes in inflammatory factors using a cytological microsphere array (CBA) (Figure S4a, see online supplementary material). While IL-2, IL-10, IL-17A, IFN-γ and IL-4 remained at concentrations too low to measure, TNF expression did not significantly differ between the three treatment groups. However, IL-6 expression in the NVs treatment group was significantly lower than in the PBS and Exos groups (Figure 5i–k and Figure S4b, see online supplementary material). In summary, these findings demonstrate that engineered NVs derived from activated neutrophils possess molecular debridement ability and promote infectious wound healing.

NVs facilitate infectious wound healing through long-term anti-inflammatory effects

To investigate the long-term effects of NVs, all rats were sacrificed on the 15th day (Figure 6). Haematoxylin and eosin (H&E) and Masson staining, as well as immunostaining for TNF-α and vascular growth factor, were conducted. The unorganized granulation tissue in the NVs group was the smallest among all the groups (Figure 6a), indicating the most effective healing. Furthermore, collagen deposition at the wound site, a critical indicator of the wound was assessed using Masson trichrome staining. The NVs-treated group showed a large area of intense blue staining compared to other groups (Figure 6b, e), indicating a dense collagen deposition at the wound site. All the results collectively confirm the efficiency of NVs in promoting wound healing. As TNF-α is a pro-inflammatory factor reflecting the level of infection-induced inflammation in wound healing [21], its expression across groups was compared. TNF-α expression in the control and Exos groups was significantly higher than that in the NVs group (Figure 6c, f), signifying the presence of inflammation at the wound site. Additionally, vascular endothelial growth factor immunostaining demonstrated that the NVs group exhibited significantly higher expression than the control and Exos groups (Figure 6d, g), indicating enhanced angiogenesis, a crucial factor in wound healing.

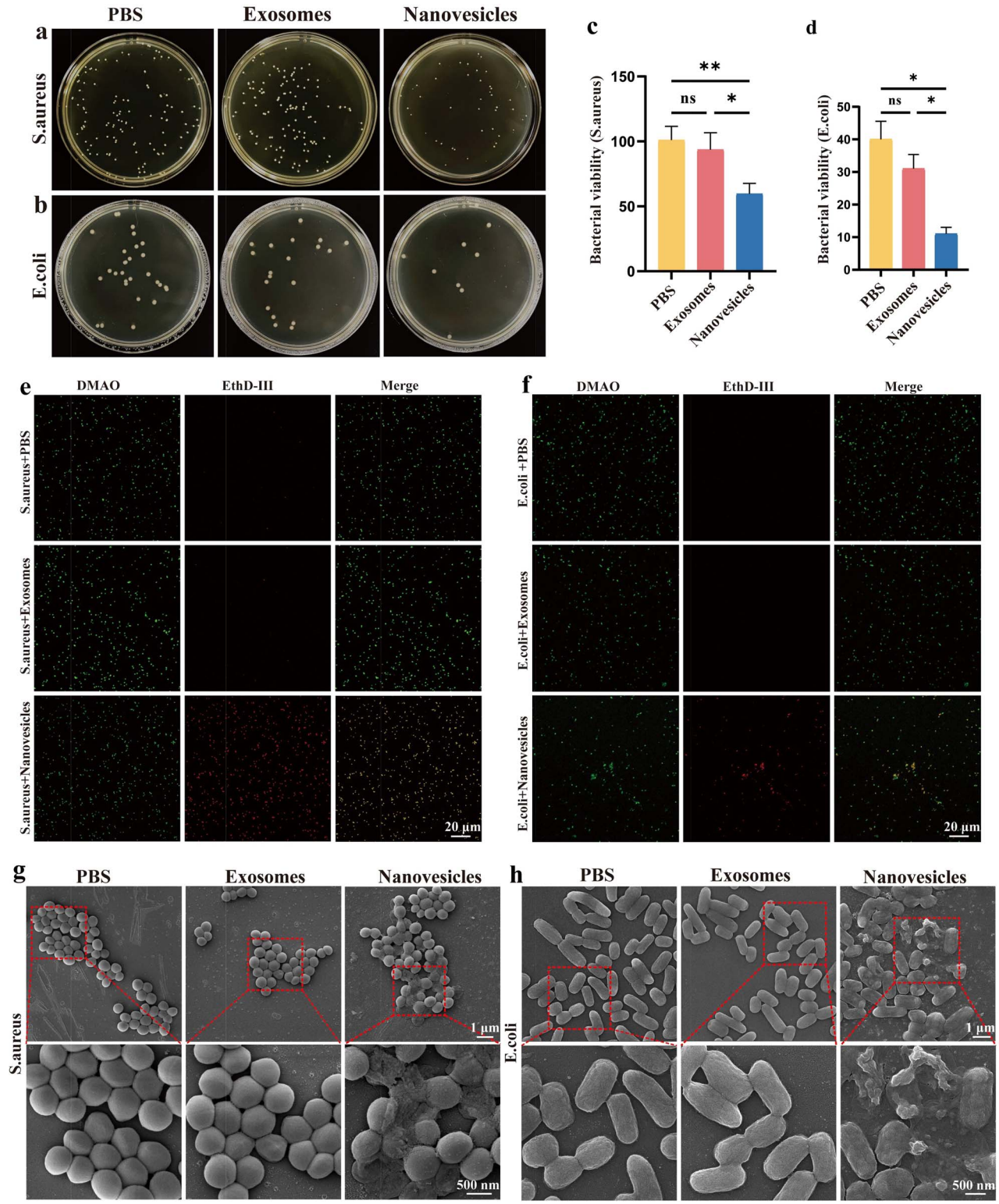

Figure 3. Bactericidal effect of nanovesicles (NVs) *in vitro*. (**a**–**d**) Bacterial colonies and bactericidal effects of PBS, exosomes (Exos) and NVs co-incubated with *Staphylococcus aureus* and *Escherichia coli* (n = 3). (**e**, **f**) Fluorescent images of *E. coli* and *S. aureus* using the LIVE/DEAD BacLight bacterial viability kit (n = 3). (**g**, **h**) Scanning electron microscopy images of *S. aureus* and *E. coli* treated with different methods (n = 3). Data are presented as mean ± SD. $^{*}p < 0.05$, $^{**}p < 0.01$; *ns*, not significant

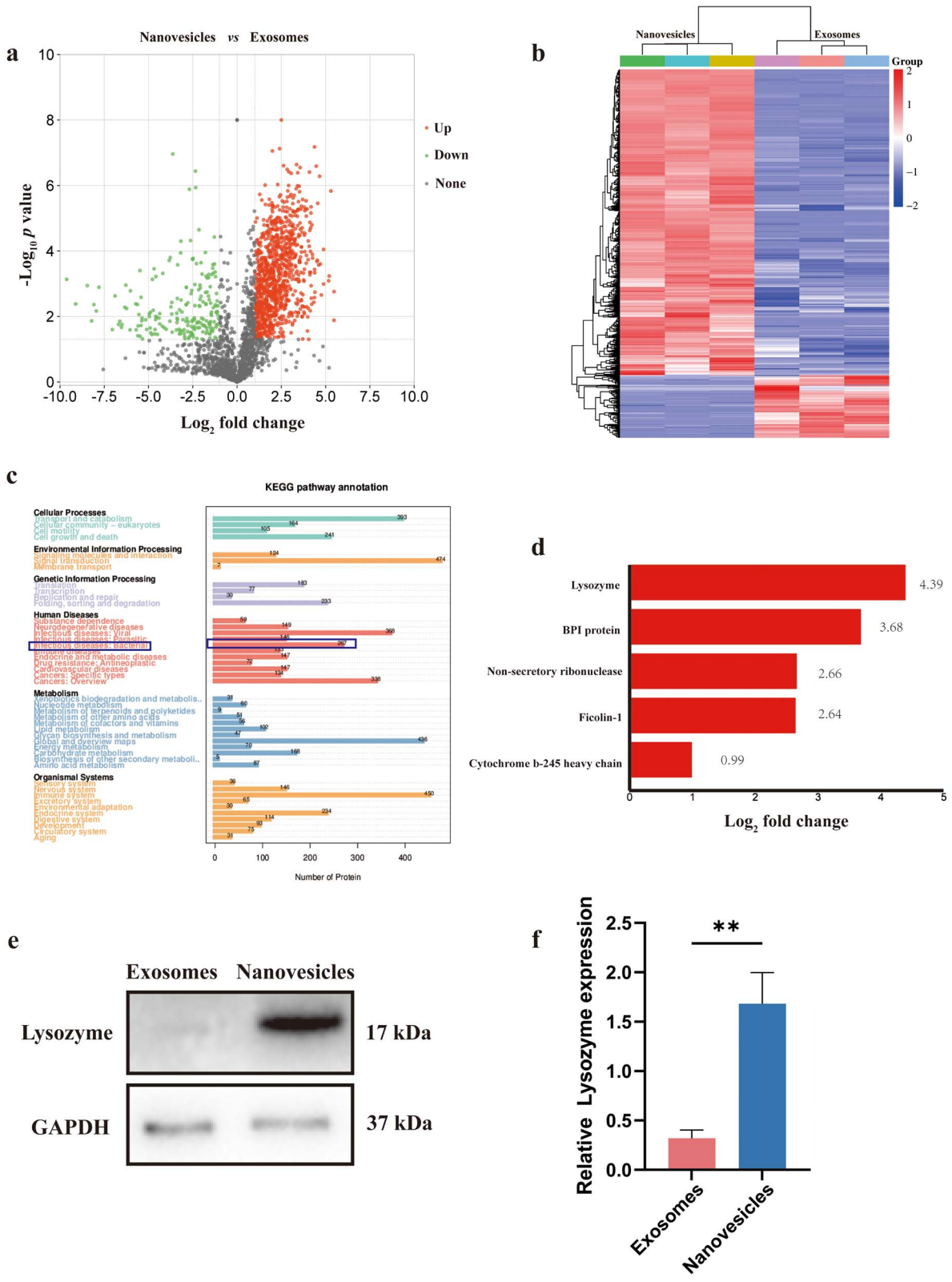

Figure 4. Proteomic analysis of nanovesicles (NVs) and exosomes (Exos). (**a**) Volcano plot depicting differential proteins between NVs and Exos. (**b**) Heatmap displaying protein levels in NVs and Exos. (**c**) KEGG analysis of proteins in NVs and Exos. (**d**) Expression of bactericidal-related proteins is significantly increased in NVs. (**e, f**) Western blot verification of lysozyme protein levels in NVs and Exos (n = 3). Data are presented as mean ± SD. $^{**}p < 0.01$. *KEGG* Kyoto Encyclopedia of Genes and Genomes, *GAPDH* glyceraldehyde-3-phosphate dehydrogenase

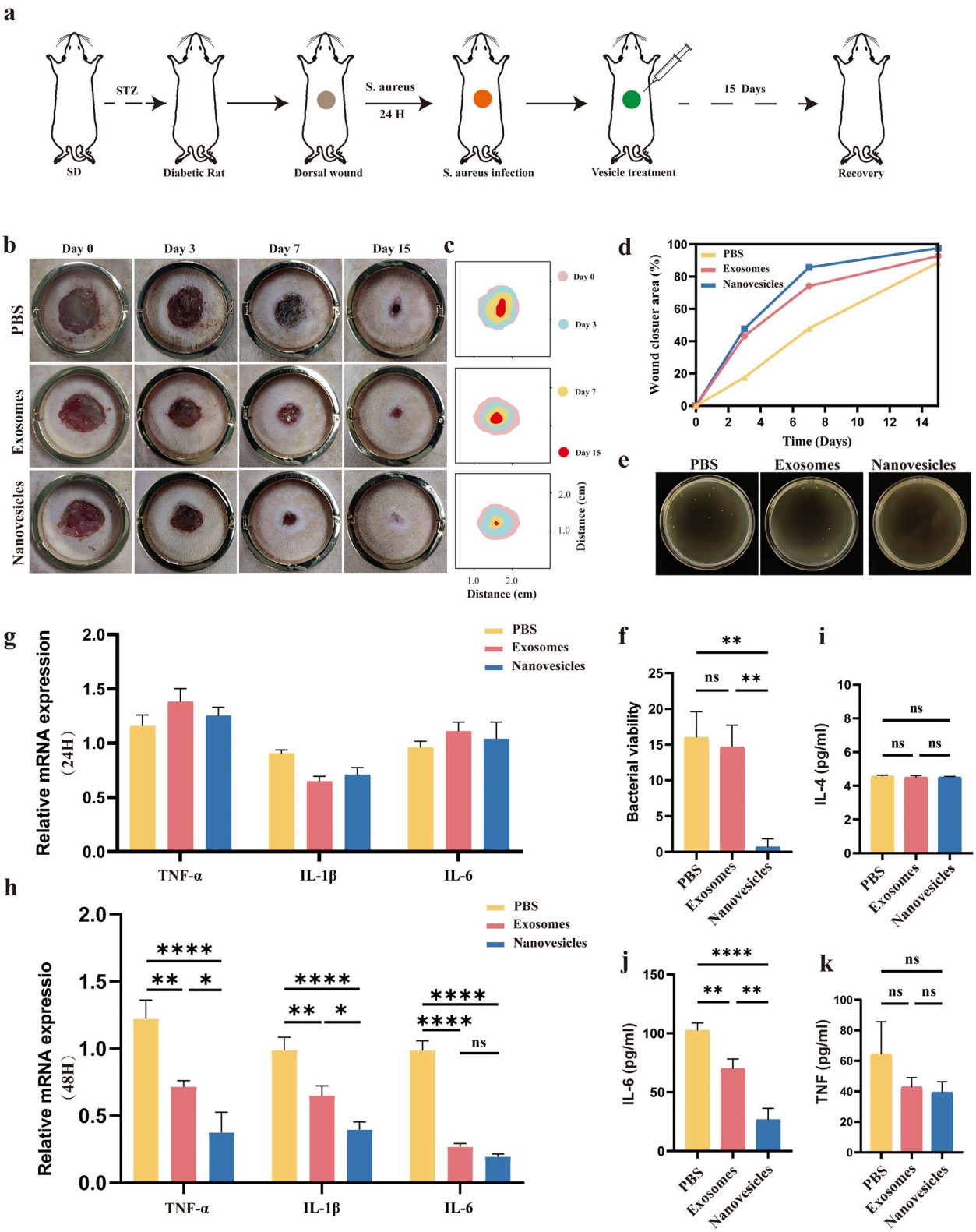

Figure 5. NVs exhibit bactericidal and anti-inflammatory effects in the acute phase of infectious wound healing. (**a**) Experimental set-up demonstrating the promotion of wound healing by NVs in diabetic rats infected with *S. aureus*. (**b**, **c**) Photographs of rat wounds at different time points following various treatments (scale bar, 10 mm). (**d**) Quantitative analysis of relative wound areas at different time points (n = 6). (**e**, **f**) Bacterial viability and corresponding photographs of bacterial colonies of *S. aureus* on LB agar plates in the wounds at 48 h post-treatments (n = 3). (**g**, **h**) Expression of inflammatory factors IL-1β, TNF-α and IL-6 in wound tissue at 24 and 48 h post-treatment (n = 3). (**i**–**k**) Expression of inflammatory factors IL-4, IL-6 and TNF in plasma at 48 h post-treatment. Data are presented as mean ± SD. $^{*}p < 0.05$, $^{**}p < 0.01$, $^{****}p < 0.0001$; *ns* not significant, *STZ* Streptozotocin, *TNF-α* tumour necrosis factor-alpha, *IL-1β* interleukin-1 beta, *IL-6* interleukin-6

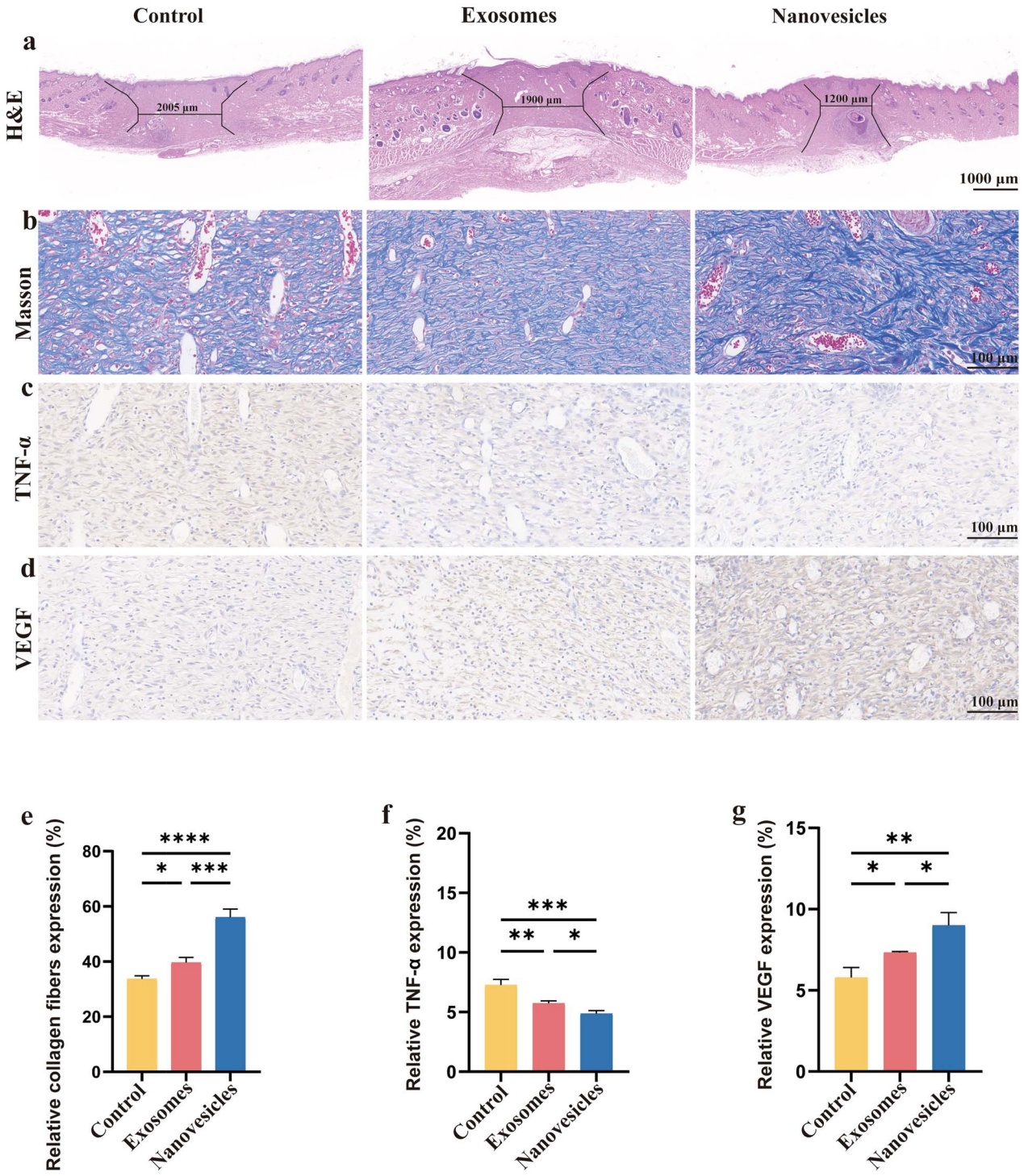

Figure 6. Nanovesicles (NVs) promote the healing of infectious wounds through long-term anti-inflammatory effects. (**a**–**d**) Hematoxylin and eosin (H&E) staining, Masson staining and immunohistochemical staining of TNF-α and VEGF were performed on wound tissue on the 15th day. (**e**–**g**) Relative expression of collagen fibers, TNF-α and VEGF were estimated (n = 3). Data are presented as mean ± SD. $^{*}p < 0.05$, $^{**}p < 0.01$, $^{***}p < 0.001$, $^{****}p < 0.0001$. *Masson* Masson's trichrome stain, *TNF-α* tumour necrosis factor-alpha, *VEGF* vascular endothelial growth factor

Discussion

In this study, we engineered NVs derived from activated neutrophils to enhance the process of infectious wound healing through debridement. Initially, we successfully isolated neutrophils from peripheral blood and activated them *in vitro* through PMA stimulation, demonstrating that activated neutrophils rapidly release a substantial amount of bactericidal proteins. We also devised a high-yield process for fabricating

NVs via extrusion, introducing a novel delivery tool to replace Exos. Our strategy enabled engineered NVs loaded with bactericidal proteins to achieve significant bactericidal effects, effectively eliminating bacterial growth in the deep tissues of infectious wounds. These findings not only underline the role of engineered NVs derived from activated neutrophils in bactericidal activity but also introduce a novel debridement method.

Bacterial infection often leads to reduced nutrient supply and insufficient oxygenation in wounds, accelerating and aggravating the pathology of various wound types, particularly diabetic wounds [22]. Bacterial colonization in deep tissues frequently results in elevated protease levels and proinflammatory cytokines, directly initiating and sustaining the inflammatory cascade [23]. Moreover, in the context of diabetic wounds, hyperglycemia and microenvironment disturbances in the affected area further impede the wound-healing process. Consequently, addressing infection and regulating the immune microenvironment are pivotal aspects of the treatment of infected wounds [24]. The increasing prevalence of antibiotic-resistant bacteria in wounds, particularly Gram-negative strains, underscores the limitations of conventional antibiotics in eliminating biofilms produced by these resistant bacteria [25]. This often leads to persistent inflammatory responses and delayed healing processes [26].

Previous studies demonstrated the potent antibacterial role of neutrophil-derived microvesicles [27]. Targeted delivery can enhance local therapeutic concentrations while minimizing side effects. In alignment with these studies, our engineered NVs from activated neutrophils exhibited high bactericidal capabilities. Bioinspired engineered NVs have been developed for wound therapy [28]. For instance, Han *et al*. [29] have developed mesenchymal stem cell-derived NVs that can promote fibroblast proliferation and thus promote skin wound healing. In addition, Jang *et al*. [15] have generated high quantities of engineered NVs from mononuclear/macrophages that not only had similar properties to Exos but also had 100-fold higher production yield. The use of nanoparticles coated with neutrophil cell membranes as a biomimetic drug delivery system and neutrophils as a living cell drug delivery system have been tested as novel strategies for various diseases [30–32]. Here, we produced engineered NVs and used them as nanocarriers for bactericidal proteins.

Proteomic analysis showed that the lysozyme content of engineered NVs was significantly higher than that of Exos. This variation in proteomic composition can be attributed to their different biogenesis, as previously stated. Exos form through the endosomal system or are shed from the plasma membrane [33], whereas the engineered NVs might encapsulate their contents through a non-selective process originating from their parent cells. Lysozyme is a naturally derived glycosidic bond-cleaving enzyme, known for its bactericidal properties primarily attributed to *N*-acetylmuramoylhydrolase enzymic activity, resulting in peptidoglycan hydrolysis and bacterial lysis [34]. As a result, lysozyme has bactericidal and bacteriostatic properties, especially against gram-positive bacteria, and its clinical application is believed to carry a low risk of inducing resistance [35].

To validate the effectiveness of engineered NVs in promoting wound healing, we established a diabetic infectious wound model by implanting *S. aureus* into wounds created on the backs of STZ-induced diabetic rats. The effective delivery of engineered NVs to deeper tissues via multipoint injection enabled pathogen eradication. We observed a significant acceleration in wound healing, downregulation of inflammatory factors and enhanced collagen deposition in wounds treated with this approach. In summary, engineered NVs derived from activated neutrophils, with their robust bactericidal properties, hold substantial promise for infectious wound healing. As part of the ongoing progression of cell-free therapy, the expanding production of NVs can enhance the treatment of diseases that require significant quantities of cells or medications to function effectively, such as diabetes and infectious wounds.

Limitations

Our studies have substantiated the bactericidal ability of engineered NVs to precisely and effectively promote infectious wound healing, offering a promising avenue for clinical wound repair. Nonetheless, challenges persist in terms of the quality, purity and yield of the prepared NVs, as well as the storage conditions of loaded engineered NVs [36]; the possible side effects of systemic use of vesicles as therapeutic agents should also be considered, all of which require further refinement [37].

Conclusions

In conclusion, we developed engineered NVs derived from activated neutrophils to serve as a novel debridement method targeting bacteria in deep tissues, ultimately promoting infectious wound healing. Engineered NVs also hold potential as effective therapeutic carriers for various agents beyond bactericidal proteins. Future developments of engineered NVs derived from neutrophils may find clinical applicability in addressing numerous human diseases including infectious wounds.

Supplementary data

Supplementary data is available at *Burns & Trauma Journal* online.

Abbreviations

Exos: Exosomes; NVs: Nanovesicles; IL: Interleukin; TNF-α: Tumour necrosis factor-alpha; STZ: Streptozotocin.

Funding

This work was supported by National Natural Science Foundation of China (No. 82072217, 81772135 and U21A20370).

Authors' contributions

HJ and BS conceived and designed the studies. XW, RS and Y Yu performed most of the experiments and analyzed the data. Y Yang, LL, ZG and RS performed some of the animal studies and assisted with the experimental design and data analyses. HJ and BS wrote the manuscript. All the authors read and revised the manuscript.

Ethical approval

This study received approval from the Medical Ethical Committee of Suzhou Municipal Hospital (KL901390). Blood specimens were collected from the cubital veins of healthy drug-free donors who provided written informed consent before participating. All experimental procedures were conducted in strict compliance with approved guidelines. All experimental procedures involving rats and mice were carried out in strict accordance with the recommendations outlined in the Guide for the Care and Use of Laboratory Animals of the National Institutes of Health and State Key Laboratory of Pathogens and Biosecurity of the Institute of Microbiology and Epidemiology.

Conflict of interest

None declared.

Data availability

The data are available within the paper or are available from the authors upon request.

References

1. Verdolino DV, Thomason HA, Fotticchia A, Cartmell S. Wound dressings: curbing inflammation in chronic wound healing. *Emerg Top Life Sci*. 2021;5:523–37.
2. Leaper D, Assadian O, Edmiston CE. Approach to chronic wound infections. *Br J Dermatol*. 2015;173:351–8.
3. Bassetti M, Peghin M, Castaldo N, Giacobbe DR. The safety of treatment options for acute bacterial skin and skin structure infections. *Expert Opin Drug Saf*. 2019;18:635–50.
4. Daeschlein G. Antimicrobial and antiseptic strategies in wound management. *Int Wound J*. 2013;10:9–14.
5. Frieri M, Kumar K, Boutin A. Antibiotic resistance. *Journal of Infection and Public Health*. 2017;10:369–78.
6. Madhok BM, Vowden K, Vowden P. New techniques for wound debridement. *Int Wound J*. 2013;10:247–51.
7. Dayya D, O'Neill OJ, Huedo-Medina TB, Habib N, Moore J, Iyer K. Debridement of diabetic foot ulcers. *Adv Wound Care (New Rochelle)*. 2022;11:666–86.
8. Lehrer RI, Ganz T, Selsted ME, Babior BM, Curnutte JT. Neutrophils and host Defense. *Ann Intern Med*. 1988;109:127–42.
9. Sun BW, Huang JM. Re-understanding the physiological and pathophysiological roles of neutrophils. *Zhonghua Shao Shang Yu Chuang Mian Xiu Fu Za Zhi*. 2022;38:109–13.
10. Shao Y, Guo Z, Yang Y, Liu L, Huang J, Chen Y, *et al.* Neutrophil extracellular traps contribute to Myofibroblast differentiation and scar hyperplasia through the toll-like receptor 9/nuclear factor kappa-B/Interleukin-6 pathway. *Burns Trauma*. 2022;10:tkac044.
11. Liew PX, Kubes P. The Neutrophil's role during health and disease. *Physiol Rev*. 2019;99:1223–48.
12. Kalluri R, LeBleu VS. The biology, function, and biomedical applications of exosomes. *Science*. 2020;367:eaau6977.
13. Wang H, Zang J, Zhao Z, Zhang Q, Chen S. The advances of neutrophil-derived effective drug delivery systems: a key review of managing Tumors and inflammation. *IJN*. 2021;16:7663–81.
14. Jo W, Kim J, Yoon J, Jeong D, Cho S, Jeong H, *et al.* Large-scale generation of cell-derived Nanovesicles. *Nanoscale*. 2014;6:12056–64.
15. Jang SC, Kim OY, Yoon CM, Choi D-S, Roh T-Y, Park J, *et al.* Bioinspired exosome-mimetic Nanovesicles for targeted delivery of chemotherapeutics to malignant Tumors. *ACS Nano*. 2013;7:7698–710.
16. Jo W, Jeong D, Kim J, Cho S, Jang SC, Han C, *et al.* Microfluidic fabrication of cell-derived Nanovesicles as endogenous RNA carriers. *Lab Chip*. 2014;14:1261–9.
17. Gheibi S, Kashfi K, Ghasemi A. A practical guide for induction of Type-2 diabetes in rat: incorporating a high-fat diet and Streptozotocin. *Biomed Pharmacother*. 2017;95:605–13.
18. Damascena HL, Silveira WAA, Castro MS, Fontes W. Neutrophil activated by the famous and potent PMA (Phorbol Myristate acetate). *Cells*. 2022;11:2889.
19. Yang Y, Liu L, Guo Z, Li L, Shao Y, Song M, *et al.* Investigation and assessment of neutrophil dysfunction early after severe burn injury. *Burns*. 2021;47:1851–62.
20. Li X, Gui R, Li J, Huang R, Shang Y, Zhao Q, *et al.* Novel multifunctional silver nanocomposite serves as a resistance-reversal agent to synergistically combat Carbapenem-resistant *Acinetobacter Baumannii*. *ACS Appl Mater Interfaces*. 2021;13:30434–57.
21. Wang Y, Sun Y, Li W, Tian W, Irini A. High performance of Nanoscaled Fe2O3 Catalyzing UV-Fenton under neutral condition with a low stoichiometry of H2O2: kinetic study and mechanism. *Chem Eng J*. 2015;267:1–8.
22. Zhao H, Huang J, Li Y, Lv X, Zhou H, Wang H, *et al.* ROS-scavenging hydrogel to promote healing of bacteria infected diabetic wounds. *Biomaterials*. 2020;258:120286.
23. Schreml S, Szeimies RM, Prantl L, Karrer S, Landthaler M, Babilas P. Oxygen in acute and chronic wound healing. *Br J Dermatol*. 2010;163:257–68.
24. Zhong Y, Seidi F, Wang Y, Zheng L, Jin Y, Xiao H. Injectable chitosan hydrogels tailored with antibacterial and antioxidant dual functions for regenerative wound healing. *Carbohydr Polym*. 2022;298:120103.
25. Diban F, Di Lodovico S, Di Fermo P, D'Ercole S, D'Arcangelo S, Di Giulio M, *et al.* Biofilms in chronic wound infections: innovative antimicrobial approaches using the In vitro Lubbock chronic wound biofilm model. *Int J Mol Sci*. 2023;24:1004.
26. Zhang Y, Wang S, Yang Y, Zhao S, You J, Wang J, *et al.* Scarless wound healing programmed by Core-Shell microneedles. *Nat Commun*. 2023;14:3431.
27. Timár CI, Lőrincz ÁM, Csépányi-Kömi R, Vályi-Nagy A, Nagy G, Buzás EI, *et al.* Antibacterial effect of microvesicles released from human neutrophilic granulocytes. *Blood*. 2013;121:510–8.
28. Yang B, Lin Y, Huang Y, Zhu N, Shen Y-Q. Extracellular vesicles modulate key signalling pathways in refractory wound healing. *Burns. Trauma*. 2023;11:tkad039.
29. Han C, Jeong D, Kim B, Jo W, Kang H, Cho S, *et al.* Mesenchymal stem cell engineered Nanovesicles for accelerated skin wound closure. *ACS Biomater Sci Eng*. 2019;5:1534–43.
30. Chu D, Dong X, Shi X, Zhang C, Wang Z. Neutrophil-based drug delivery systems. *Adv Mater*. 2018;30:e1706245.
31. Che J, Najer A, Blakney AK, McKay PF, Bellahcene M, Winter CW, *et al.* Neutrophils enable local and non-invasive liposome

delivery to inflamed skeletal muscle and ischemic heart. *Adv Mater*. 2020;32:e2003598.
32. Zhang J, Ji C, Zhang H, Shi H, Mao F, Qian H, *et al.* Engineered neutrophil-derived exosome-like vesicles for targeted cancer therapy. *Sci Adv*. 2022;8:eabj8207.
33. Van Niel G, D'Angelo G, Raposo G. Shedding light on the cell biology of extracellular vesicles. *Nat Rev Mol Cell Biol*. 2018;19:213–28.
34. Ragland SA, Criss AK. From bacterial killing to immune modulation: recent insights into the functions of lysozyme. *PLoS Pathog*. 2017;13:e1006512.
35. Chen L-L, Shi W-P, Zhang T-D, Zhou Y-Q, Zhao F-Z, Ge W-Y, *et al.* Antibacterial activity of lysozyme-loaded cream against MRSA and promotion of scalded wound healing. *Int J Pharm*. 2022;627:122200.
36. Ye H, Wang F, Xu G, Shu F, Fan K, Wang D. Advancements in engineered exosomes for wound repair: current research and future perspectives. *Front Bioeng Biotechnol*. 2023;11:1301362.
37. Genschmer KR, Russell DW, Lal C, Szul T, Bratcher PE, Noerager BD, *et al.* Activated PMN exosomes: pathogenic entities causing matrix destruction and disease in the lung. *Cell*. 2019;176:113–126.e15.